Insights into the Charge-Transfer Character of Electronic Transitions in $^{R}Cp_2Ti(C_2Fc)_2$ Complexes Using Solvatochromism, Resonance Raman Spectroscopy, and TDDFT

Journal:	*Dalton Transactions*
Manuscript ID	DT-ART-12-2020-004282.R1
Article Type:	Paper
Date Submitted by the Author:	15-Jan-2021
Complete List of Authors:	Carlton, Elizabeth; Furman University, Department of Chemistry Sutton, Joshua; Otago University, School of Chemistry Gale, Ariel; Furman University, Department of Chemistry Shields, George; Furman University, Provost's Office & Department of Chemistry Gordon, Keith; University of Otago, Chemistry Wagenknecht, Paul; Furman University, Department of Chemistry

Insights into the Charge-Transfer Character of Electronic Transitions in $^RCp_2Ti(C_2Fc)_2$ Complexes Using Solvatochromism, Resonance Raman Spectroscopy, and TDDFT

Elizabeth S. Carlton,[a] Joshua J. Sutton,[b] Ariel G. Gale,[a] George C. Shields,[a] Keith C. Gordon,[b] and Paul S. Wagenknecht[a],*

[a] Department of Chemistry, Furman University, Greenville, SC, 29613 USA
[b] Department of Chemistry, University of Otago, P.O. Box 56, Dunedin, New Zealand

Abstract A series of complexes with low-energy Fe^{II} to Ti^{IV} metal-to-metal charge-transfer (MMCT) transitions, $Cp_2Ti(C_2Fc)_2$, $Cp^*_2Ti(C_2Fc)_2$, and $^{MeOOC}Cp_2Ti(C_2Fc)_2$, was investigated using solvatochromism and resonance Raman spectroscopy (RRS) augmented with time-dependent density functional theory (TDDFT) calculations in order to interrogate the nature of the CT transitions. Computational models were benchmarked against the experimental UV-Vis spectra and B3LYP/6-31G(d) was found to most faithfully represent the spectra. The energy of the MMCT transition was measured in 15 different solvents and a multivariate fit to the Catalán solvent parameters - solvent polarizability (SP), solvent dipolarity (SdP), solvent basicity (SB), and solvent acidity (SA) - was performed. The effect of SP indicates a greater degree of electron delocalization in the excited state (ES) than the ground state (GS). The small negative solvatochromism with respect to SdP indicates a smaller dipole moment in the ES than the GS. The effect of SB is consistent with charge-transfer to Ti. Upon excitation into the MMCT absorption band, the RRS data show enhancement of the alkyne stretching modes and of the out-of-plane bending modes of the cyclopentadienyl ring connected to Fe and the alkyne bridge. This is consistent with changes in the oxidation states of Ti and Fe, respectively. The higher-energy transitions (350 – 450 nm) show enhancement of vibrational modes consistent with ethnylcyclopentadienyl to Ti ligand-to-metal charge transfer (LMCT). The RRS data is consistent with the TDDFT predicted character of these transitions. TDDFT suggests that the lowest-energy transition in $Cp_2Ti(C_2Fc)_2CuI$, where CuI is coordinated between the alkynes, retains its Fe^{II} to Ti^{IV} MMCT character, in agreement with the RRS data, but that the lowest-energy transitions have significant CuI to Ti character. For $Cp_2Ti(C_2Fc)_2CuI$, excitation into the low-energy MMCT absorption band results in selective enhancement of the symmetric alkynyl stretching mode.

Introduction

　　Donor π-bridge acceptor (D-π-A) complexes have been thoroughly investigated for the past several decades due to possible applications in the fields of solar energy conversion[1-4] and nonlinear optical materials.[5-9] Both of these applications take advantage of low-energy charge-transfer (CT) absorptions with high molar absorptivities. We have recently investigated the charge-transfer behavior of titanocenes with an alkynyl bridge between a donor such as ferrocene (Fc)[10-12] or an arylamine[13] and the Ti^{IV} acceptor (Figure 1). Spectroscopic, electrochemical, and computational investigations demonstrated that the intense low-energy (LE) absorption for these complexes involves CT to Ti^{IV}.
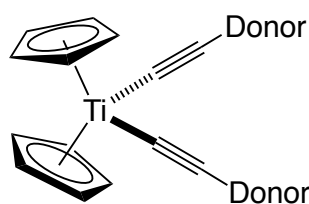
Figure 1. General structure of titanocenes with strong CT bands. Donors studied have included ferrocene, dimethylaniline, and triphenylamine.

　　The solvatochromism of materials whose absorption spectra are dominated by charge-transfer bands is often used to gain further understanding into the nature of the charge transfer.[14-17] Previously, the solvatochromism of the Fe^{II} to Ti^{IV} metal-to-metal charge-transfer (MMCT) band in complexes with a Fc donor and titanocene acceptor was investigated with a small set of solvents.[10] The dominant solvent parameter affecting the absorption energy appeared to be solvent polarizabilty, with solvent dipolarity appearing to have very little impact on the energy of this CT band.   Even though solvent polarizability provided the best fit to any single parameter model, and also better than multivariate fits using the Kamlet and Taft model,[16] several solvents were clear outliers.

To further investigate the character of the CT transitions and the impact of solvent on these transitions, we have chosen a set of complexes whose electron density at Ti^{IV} is systematically varied through substitution at the cyclopentadienyl ring, $Cp*_2Ti(C_2Fc)_2$, $Cp_2Ti(C_2Fc)_2$, and $^{MeOOC}Cp_2Ti(C_2Fc)_2$ (Figure 2). The
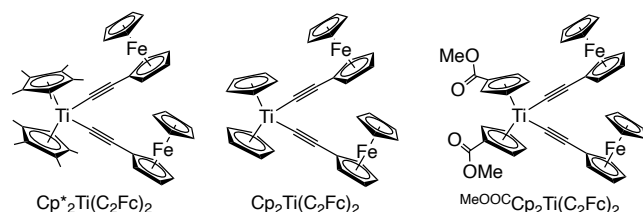
Figure 2. Structures and abbreviations for the three complexes investigated herein.

impact of the substitution at Cp is clearly observed in the $Ti^{IV/III}$ reduction potentials which range from -2.28 V for the electron rich Cp* complex, to -1.75 V for the Cp complex, to -1.46 V (vs $Fc^{+/0}$) for the ^{MeOOC}Cp complex, the latter being a result of the electron withdrawing ester substituents.[10-11] This anodic shift as the cyclopentadienyl ring becomes more electron poor (left to right in Figure 2) results in a concomitant red-shift of the LE absorption band for these complexes (540 – 630 nm, Figure 3). A Marcus-Hush type analysis of the electrochemical and
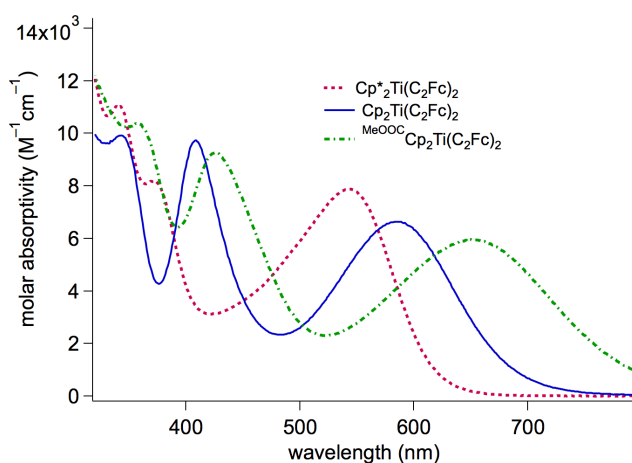
Figure 3. UV-Visible spectra of complexes with Fe^{II} to Ti^{IV} MMCT in CH_2Cl_2. Replacement of Cp with the more electron-rich Cp* shifts the MMCT to higher energy, whereas replacement of Cp with the more electron-poor ^{MeOOC}Cp shifts the MMCT to lower energy.

4

spectroscopic data is consistent with the assignment of the LE absorption as an Fe^{II} to Ti^{IV} MMCT band. Chiefly, good agreement was observed between $\Delta E_{1/2}$ ($E_{1/2}$ $Fc^{+/0}$ − $E_{1/2}$ ($Ti^{IV/III}$)) and the spectroscopically determined value for $\Delta G°$. Time-dependent density functional theory (TDDFT) has supported the MMCT character of the LE absorption but with some Fe-centered d-d character mixed in.[10-11] Furthermore, TDDFT demonstrates that both the density of charge transferred (Q_{CT}) and the distance between the barycenters for charge depletion and accumulation (D_{CT}) increase with the anodic shift of the $Ti^{IV/III}$ potential.[11] Both would contribute to a larger shift in the dipole associated with the LE absorption and may impact the degree to which solvent dipolarity impacts the absorption spectrum. In an attempt to further understand the character of the CT excited states, we report a systematic analysis of the TDDFT, solvatochromism, and Resonance Raman spectroscopy (RRS) of all three complexes.

Solvatochromism will be used to determine if the direction of the dipole moment changes are consistent with the understanding of the MMCT. Likewise, in RRS the enhancement of Raman bands associated with the resonance effect provides insight into the structural distortions concomitant with the resonant photoexcitation.[18-20] That is to say, that the vibrational modes that mimic the structural changes associated with exciting into a particular state will show stronger enhancement than those vibrational bands with modes that do not mimic the excited state structure,[19-23] thus allowing for more complete assignment of the electronic transitions. DFT and TDDFT also give descriptions of the electronic transitions and the ground- and excited-state dipole moments and thus are used to aid in interpreting the solvatochromism. Herein, we find good agreement between theoretical and experimental descriptions of the dipole moment changes and orbitals involved in the transitions. The aggregated results are consistent with a

MMCT transition to Ti^{IV} from a donor MO that is delocalized across both ethynylferrocene ligands.

Experimental

Materials and Methods: THF, Et$_2$O, and CH$_2$Cl$_2$ were dried and degassed using an Innovative Technology Inc. solvent purification system before use. All other solvents were reagent grade and used as received. Cp$_2$Ti(C$_2$Fc)$_2$, Cp*$_2$Ti(C$_2$Fc)$_2$, ^{MeOOC}Cp$_2$Ti(C$_2$Fc)$_2$, and Cp$_2$Ti(C$_2$Fc)$_2$CuI were prepared according to the literature procedures.[10-12] UV-Visible absorption spectra were recorded using a Cary-50 spectrophotometer with the cell holder thermostated to 20 ˚C. Resonance Raman spectra were collect using a 135° illumination backscattering setup as previously described,[24] in short, krypton ion (Innova 300C, Coherent Inc., USA) or diode lasers (Cobolt, Sweden and Crystal Laser, USA) were used for excitation, matching notch- or long-pass-filters (Kaiser Inc., USA) were used to block the Rayleigh line and the spectrum was dispersed on to a Pylon 400BRX CCD (Princeton Instruments, USA) using an Isoplane SCT320 spectrometer (Princeton Instruments, USA). Gaussian 16[25] was used for all DFT and TDDFT calculations. For each computational model, the geometry was optimized and the structure checked to be a minimum based on the frequency calculation. TDDFT was performed for each model at the same level of theory as the optimization. GaussView 6[26] was used for all orbital imaging. GaussSum 3[27] was used for Mulliken population analysis.

Results and Discussion

Computational Model

Interpretation of solvatochromism and RRS is significantly enhanced by DFT and TDDFT, thus, we have continued to refine the computational model for this series of complexes. Previously, the B3PW91/6-311+G(d) model (chosen based on success of the model with other

D-π-A systems with Fc donors[7]) was shown to faithfully represent the low-energy MMCT transition in the electronic spectra (TDDFT), whereas the more sophisticated range-separated hybrid and meta-hybrid functionals ωB97XD, CAM-B3LYP, and M06-2X do not.[10-11] We continued to investigate additional models, with initial screening focusing on $Cp_2Ti(C_2Fc)_2$. For the sake of comparison with recent calculations,[11] the medium was represented by a Tomasi polarizable continuum model (PCM)[28] assigned the macroscopic dielectric constant of THF. Because the B3LYP/6-31G(d) model has been shown to successfully model the electronic spectra of ferrocene[29] and transition-metal complexes with CT absorptions,[30] we further investigated this model. Indeed, it represents the electronic spectrum of $Cp_2Ti(C_2Fc)_2$ at least as faithfully as the more computationally expensive B3PW91/6-311+G(d) model (Table 1, and ESI Figure S1). Neither B3PW91 with the smaller 6-31G(d) basis, nor B3LYP with the larger 6-

Table 1. Lowest energy (LE) singlet transition for various computational models for $Cp_2Ti(C_2Fc)_2$[a]

Model	λ (LE transition)
Experimental[b]	571 nm
B3PW91/6-311+G(d)	562 nm
B3LYP/6-31G(d)	576 nm
B3PW91/6-31G(d)	541 nm
B3LYP/6-311+G(d)	617 nm
B3LYP/def2tzv/tzvpfit	677 nm
B3LYP/6-31G(d)/LANL2DZ[c]	625 nm
B3LYP/6-31G(d) gd3bj[d]	557 nm
B3LYP/6-31G(d) gd3bj[d] lanl2[e]	522 nm

[a] All models include solvent=thf. [b] λ_{max} in THF. [c] Split valence set with LANL2DZ for Ti and Fe. [d] empiricaldispersion=gd3bj. [e] pseudo(lanl2).

311+G(d) basis represented the spectrum as well as B3LYP/6-31G(d). B3LYP was also investigated using either the def2tzv or the split-valence 6-31G(d)/LANL2DZ basis sets, neither of which improved the performance vs B3LYP/6-31G(d). Furthermore, the addition of empirical dispersion and pseudo core potentials also did not improve upon B3LYP/6-31G(d) (Table 1, and ESI Figure S1). Lastly, B3LYP/6-31G(d) was used to predict the spectra of $Cp^*_2Ti(C_2Fc)_2$ and $^{MeOOC}Cp_2Ti(C_2Fc)_2$. Once again, agreement with experiment was at least as good as using the

more computationally expensive B3PW91/6-311+G(d) (ESI Figure S2). Consistent with prior

reports,[10, 11] the lowest-energy absorption is dominated by a HOMO to LUMO transition,

exhibiting delocalized ethynylferrocene to Ti^{IV} MMCT character (Figure 4). In addition to

reasonable agreement between B3PW91/6-311+G(d) and B3LYP/6-31G(d) in terms of

predicting the spectra of the $^RCp_2Ti(C_2Fc)_2$ complexes, there is also reasonably good agreement

between these models for the predicted S0 and S1 dipoles (vide infra).
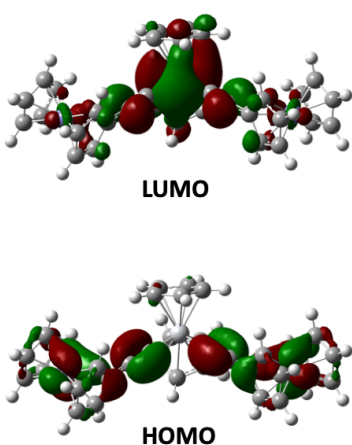
Figure 4. Frontier orbitals for $Cp_2Ti(C_2Fc)_2$ calculated using B3LYP/6-31G(d) in a THF solvent field.

Solvatochromism

Summary of Results The energies of charge-transfer transitions are often quite solvent

dependent. In particular, nonspecific solvent-solute interactions involving solvent polarity and

solvent polarizability often modify the CT energy. Likewise, specific interactions between the

solvent and analyte, where the solvent may act as a Lewis acid or Lewis base, are also often

important.[14-17] We previously reported that plotting the energy of the MMCT transition for

$Cp_2Ti(C_2Fc)_2$ against Catalán's solvent polarizability (SP)[17] scale gave the best fit of any single

solvent parameter, and even better than the Kamlet and Taft multivariate model.[10] However, in

the plot of the CT energy against SP, the chlorinated solvents and toluene were clearly outliers

(Figure 5). This encouraged the investigation of the other three Catalán solvent parameters in addition to SP, namely solvent dipolarity (SdP), solvent basicity (SB), and solvent acidity (SA).[17] Inspection of these additional three parameters for the solvents shown in Figure 5 reveal that the one solvent parameter that is significantly different for the outliers (red triangles) compared to the data points that appear to fall in line (black dots) is SB. Thus, in addition to investigating the effect of SdP, the present investigation is also intended to interrogate the impact of SB. Consequently, solvents with a wide range of both SdP and SB values were chosen. Solvent acidity is more difficult to interrogate due to the lack of solubility in solvents with SA values greater than 0.1.
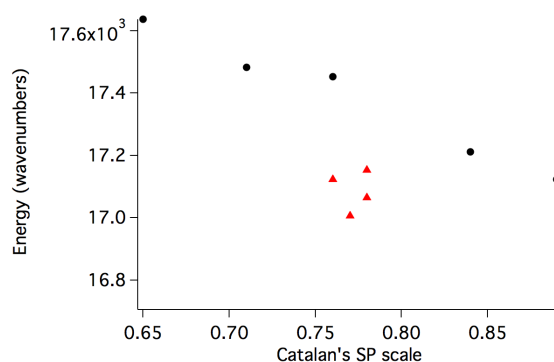
Figure 5. Energy of the MMCT transition for $Cp_2Ti(C_2Fc)_2$ as a function of Catalan's SP scale. The red triangles indicate toluene, CCl_4, $CHCl_3$, and CH_2Cl_2.

Though many solvent scales account for these four solvent properties,[16, 31-34] in the Catalán model these experimentally determined parameters have been demonstrated to be orthogonal, thus allowing for a clear separation of the effect of each solvent property.[17] Accordingly, the energy of the CT band, E, can be described using a multivariable model (eq 1) where $E°$ is the energy of the CT band in the absence of solvent effects and the coefficients a, b, c, and d, determined from multiple linear regression, describe the susceptibility of the transition energy to each of the solvent parameters.

$$E(\text{cm}^{-1}) = E° + a\text{SP} + b\text{SB} + c\text{SdP} + d\text{SA} \qquad (1)$$

Absorption spectra for all three complexes were recorded in fifteen solvents (Figure 6,

Table 2, and ESI Figures S3-S5). Initial multivariate fits were performed using all four Catalán

Table 2. Solvatochromism for Cp$_2$Ti(C$_2$Fc)$_2$, Cp*$_2$Ti(C$_2$Fc)$_2$, and ^{MeOOC}Cp$_2$Ti(C$_2$Fc)$_2$.

Solvent	SP	SB	SdP	SA	Cp$_2$Ti(C$_2$Fc)$_2$ MMCT (cm^{-1})	Cp*$_2$Ti(C$_2$Fc)$_2$ MMCT (cm^{-1})	^{MeOOC}Cp$_2$Ti(C$_2$Fc)$_2$ MMCT (cm^{-1})
Tributylamine	0.689	0.854	0.06	0	17179	18365	15576
Dodecane	0.683	0.086	0	0	17109	18315	15540
CCl$_4$	0.768	0.044	0	0	16992	18282	15337
o-dichlorobenzene	0.869	0.144	0.676	0.033	16992	18315	15186
Decalin	0.744	0.056	0	0	17050	18265	a
CHCl$_3$	0.783	0.071	0.614	0.047	17036	18382	15256
Nitrobenzene	0.891	0.240	0.873	0.056	17167	18315	15326
Heptane	0.635	0.083	0	0	17167	18365	15637
Toluene	0.782	0.128	0.284	0	17138	18315	15432
CH$_2$Cl$_2$	0.761	0.178	0.769	0.040	17109	18416	15326
Pyridine	0.842	0.581	0.761	0.033	17241	18365	15444
DMSO	0.830	0.647	1	0.072	17452	18349	15613
DMF	0.759	0.613	0.977	0.031	17513	18450	15686
THF	0.714	0.591	0.634	0	17513	18450	15686
Acetone	0.615	0.475	0.907	0	17606	18553	15785

^{a} absorbance peak not observed due to solubility. Values are +/- 50 cm^{-1}
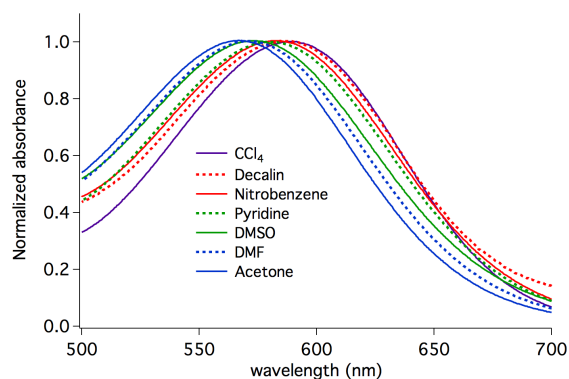
Figure 6. Effect of solvent on UV-Vis absorption spectra for Cp$_2$Ti(C$_2$Fc)$_2$. Due to peak width, location of peak maxima is +/– 1.5 nm. For clarity, only a representative subset of the solvents used in this study are included.

parameters. When a parameter was deemed not to be statistically significant (null hypothesis

accepted), the multivariate fit was performed a second time, omitting the statistically

insignificant parameter(s). Fitting this data for Cp$_2$Ti(C$_2$Fc)$_2$ according to eq 1 yields eq 2.

$$E = 18{,}030 \ (\pm 260) - 1400 \ (\pm 350) \ SP + 300 \ (\pm 100) \ SB + 330 \ (\pm 80) \ SdP \ \text{cm}^{-1} \qquad (2)$$

Figure 7 shows a graphical representation of the goodness of fit ($R^2 = 0.80$). The solvatochromic

data for $Cp^*_2Ti(C_2Fc)_2$ and $^{MeOOC}Cp_2Ti(C_2Fc)_2$ were similarly fit to eq 1 and plotted (ESI

Figures S4 – S5), and the fit parameters for all three complexes are summarized in Table 3.
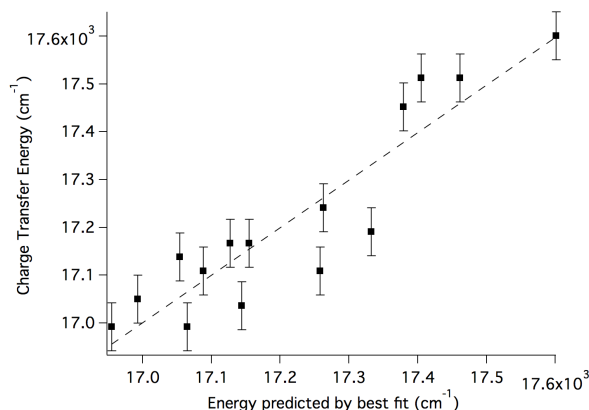
Figure 7. Energy of the experimentally determined MMCT energy plotted vs the energy predicted from eq 2

Table 3. Linear regression fit parameters and statistics

Complex	Coefficient (std error)					R^2	Adj. R^2
	intercept	SP	SB	SdP	SA		
$Cp_2Ti(C_2Fc)_2$	18030 (260)	−1400 (350)	300 (100)	330(80)	−^{a}	0.84	0.80
$Cp^*_2Ti(C_2Fc)_2$	18890 (60)	−810 (80)	−^{a}	176 (16)	−^{a}	0.93	0.92
$^{MeOOC}Cp_2Ti(C_2Fc)_2$	16440 (250)	-1420 (320)	360 (100)	−^{a}	−^{a}	0.76	0.72

^{a} The coefficients to these parameters were not statistically significant (null hypothesis accepted).

The solvatochromism for all three complexes is dominated by the effect of solvent

polarizability, with the MMCT energy decreasing with increased SP. This implies that the

excited state (ES) is more polarizable than the ground state (GS), suggesting, not surprisingly, a

greater degree of electron delocalization in the ES than the GS.[35] Both the Cp and Cp*

complexes also show an increase in transition energy with SdP. This slight negative

solvatochromism indicates that the excited state is less stabilized by polar solvents than the

ground state, suggesting a smaller dipole moment in the excited state than in the ground state.

This, in turn, suggests that the electron density shift during the MMCT transition is in the

opposite direction of the GS dipole.

Computational Investigations of S0 and S1 Dipoles To test the hypothesis that the electron density shift during the MMCT transition is in the opposite direction of the GS dipole, the S0 and S1 dipoles were calculated using DFT and TDDFT at the at the B3LYP/6-31G(d) level of theory. The computational models suggest that both $Cp_2Ti(C_2Fc)_2$ and $Cp*_2Ti(C_2Fc)_2$ have GS dipoles directed along the C_2 axis, pointing from Ti toward the two ferrocenes (Table 4, Figure 8). The change in dipole associated with Fe^{II} to Ti^{IV} MMCT is expected to be in the opposite direction.

Table 4. Computational data for S0 and S1 dipoles of titanocenes[a]

	B3PW91/6-311+G(d)		B3LYP/6-31G(d)		Δ(dipole)$_{avg}$	$Q_{CT} \times D_{CT}$[b]
	S0 dipole	S1 dipole	S0 dipole	S1 dipole		
$Cp*_2Ti(C_2Fc)_2$	3.01 D	0.46 D	3.23 D	0.48 D	2.65 D	2.77 D
$Cp_2Ti(C_2Fc)_2$	2.13 D	-1.61 D	2.26 D	-1.75 D	3.88 D	4.15 D
$^{MeOOC}Cp_2Ti(C_2Fc)_2$	-3.98 D[c]	-10.08 D[c]	-2.91 D[c]	-8.64 D[c]	5.87 D[c]	7.10 D
$^{MeOOC}Cp_2Ti(C_2Fc)_2$			0.94 D[d]	-4.65 D[d]	5.59 D[d]	

[a] All calculations run using solvent=tetrahydrofuran for comparison with reference 11. [b] From Ciofini indices Q_{CT} and D_{CT} in reference 11. Δ(dipole) = $Q_{CT} \times D_{CT} \times$ 1 Debye/0.208 eÅ. [c] Calculated using the optimized structure. [d] Calculated from simple averages of three conformations.
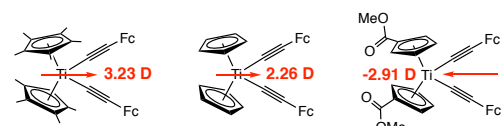
Figure 8. Ground state (S0) dipole moments calculated from the optimized structure using B3LYP/6-31G(d).

Computational results support this hypothesis; chiefly, for $Cp*_2Ti(C_2Fc)_2$, the S1 dipole is smaller but still in the same direction and for $Cp_2Ti(C_2Fc)_2$ the dipole is smaller and in the opposite direction. Because solvatochromism is dependent on the difference in magnitude of the dipole moment in the ground and excited states, and not the direction, both are consistent with a small negative solvatochromism with repect to SdP. However, the computational data is not in agreement with the slightly larger magnitude SdP coefficient for $Cp_2Ti(C_2Fc)_2$ than for $Cp*_2Ti(C_2Fc)_2$, indicating the limitations of the computational model to reveal this nuance.

The calculated GS dipole moment of the optimized structure for $^{MeOOC}Cp_2Ti(C_2Fc)_2$ points in the opposite direction than either the Cp or Cp* complexes. It is likely that this is a result of the position of the acetyl groups in the optimized structure (Figure 8). However, the

known low barrier to rotation of Cp rings on titanocenes[36] suggests that all conformations should be considered. The room-temperature ^{1}H NMR spectrum of $^{MeOOC}Cp_2Ti(C_2Fc)_2$,[11] showing only two chemically distinct protons on the substituted titanocene Cp rings is also consistent with full rotation of the Cp ligands.[37] To test the impact of the position of the ester on the dipole moment, two additional conformers with C_2 symmetry were minimized after constraining dihedral angles (Figure 9), and their S0 and S1 dipoles interrogated using the B3LYP/6-31G(d) model. Though many additional structures likely exist, these were chosen (1) to sample the conformational space and (2) because crystal structures of titanocenes with bulky substituents in these positions have been observed.[38] These three structures are within 1.4 kcal/mol of one another. Due to typical

S0 = −2.91 D	S0 = 4.29 D	S0 = 1.45 D
S1 = −8.64 D	S1 = −2.12 D	S1 = −3.2 D
min = 0 kcal/mol	1.1 kcal/mol	1.4 kcal/mol
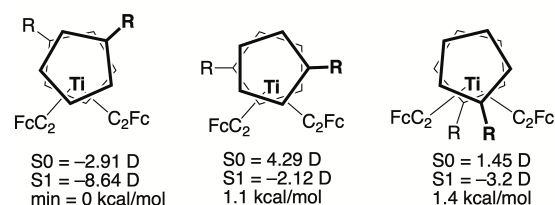
Figure 9. Top down view of three different conformers for $^{MeOOC}Cp_2Ti(C_2Fc)_2$ (where R = MeOOC). The leftmost structure is the global electronic energy minimum, representing the structure shown in Figure 8.

energy errors associated with the computational model,[39] unequivocal assignment of the lowest electronic energy structure is not possible. Though many more conformers than those shown in Figure 9 exist, a simple average of these three structures results in an S0 dipole that points in the same direction as the other two complexes. Furthermore, the transition to S1 reverses that dipole direction (Table 4). The fact that the experimental effect of SdP on the transition energy is not statistically significant for $^{MeOOC}Cp_2Ti(C_2Fc)_2$ suggests that there is either no dipole moment change from S0 to S1, or more likely that the S1 dipole is reversed in direction but with the same magnitude as S0. Certainly the directional change in dipole demonstrated from the computational model is consistent with such a conclusion, but the computational model is at present insufficient to calculate the magnitudes correctly. Thus, for all cases the calculated

directional change in dipole is consistent with the effect of SdP on transition energy, but the magnitudes of the calculated dipoles for S0 and S1 do not faithfully represent the magnitude of the effect of SdP. Lastly, it is worth noting that for all three complexes, the computational difference between S0 and S1, Δ(dipole) in Table 4, is in good agreement with Δ(dipole) determined from the product of Q_{CT} and D_{CT}.

Solvent Basicity In addition to these two nonspecific solvent interactions, both $Cp_2Ti(C_2Fc)_2$ and $^{MeOOC}Cp_2Ti(C_2Fc)_2$ show a slight dependence on the solvent basicity, indicating some region of positive charge density with which the solvent interacts. The sign of this parameter indicates that the ground state is stabilized by solvent basicity more than the excited state. Furthermore, because the Fe^{II} to Ti^{IV} MMCT excited state involves increased electron density at the titanocene and decreased density at ferrocene, and because the solvent binding must be more significant in the ground state than the excited state, this suggests that the region of positive charge density with which the solvent interacts is on the titanocene. Such a conclusion is consistent with the lack of any dependence on SB for $Cp^*_2Ti(C_2Fc)_2$, as the methyl groups on Cp* likely shield regions of positive charge density from the solvent. Another explanation for the lack of dependence on SB in the Cp* complex is that the more electron rich Cp* ligand negates any positive electron density at the titanocene with which donor solvents can interact. This is consistent with the more cathodic $Ti^{IV/III}$ potential for $Cp^*_2Ti(C_2Fc)_2$ when compared to $Cp_2Ti(C_2Fc)_2$ and $^{MeOOC}Cp_2Ti(C_2Fc)_2$.

Comparison with other Fc-π-A Complexes Solvatochromism has been reported for CT bands in many Fc-π-A complexes. For complexes where the acceptor is cationic, negative solvatochromism is typically observed,[40-44] whereas for complexes with neutral acceptors, positive solvatochromism is typically observed,[40, 42, 45-49] though some of these conclusions are

based on only two or three solvents. In some cases, analysis of extensive solvent sets results in irregular fits to any known solvent parameters.[43, 48] Of the reports that use multivariate fits to model the solvatochromic data, most use Kamlet and Taft's π^* parameter to model unspecific interactions. Because this parameter is a mixture of dipolarity and polarizability, the individual impact of each of these solvent influences is not well determined. Only one of these reports[49] uses the Catalán model. In that report, a complex with two ferrocenyl donors attached to a thiophene acceptor, 5,7-diferrocenylthieno[3,4-b]pyrazine, shows very similar solvatochromic behavior to those investigated herein. Namely, SP dominates ($a = -1540$) and there is a small negative solvatochromism with respect to SdP ($c = 301$). In this case no dependence on SB is observed but there is a slight dependence on SA ($d = 389$), probably due to hydrogen bonding to the pyrazine nitrogen atoms.

Resonance Raman Spectroscopy

Overview Resonance Raman spectra were collected for $Cp_2Ti(C_2Fc)_2$, $Cp^*_2Ti(C_2Fc)_2$, and $^{MeOOC}Cp_2Ti(C_2Fc)_2$. As discussed above, each complex displays a low-energy absorption ascribed to an Fe^{II} to Ti^{IV} MMCT. Higher energy transitions have been ascribed to LMCT transitions to Ti^{IV}.[10, 11] Thus, resonance Raman spectra were obtained over a range of excitation wavelengths in order to assist in assignment of these transitions. An additional complex with copper(I) iodide bound between the alkynes, $Cp_2Ti(C_2Fc)_2CuI$, also has a low-energy transition ascribed to an Fe^{II} to Ti^{IV} MMCT.[12] However, the presence of CuI leads to better resolution between the Raman peaks for the symmetric and asymmetric alkynyl CC. Thus, resonance Raman spectra for this complex were obtained to investigate whether either or both modes are selectively enhanced. Such observations have been used to draw conclusions regarding whether the excited state is localized or delocalized across two donors.[50] Thus, RRS can be used to test

the hypothesis that the excited state is delocalized across both Fc ligands. All resonance Raman

spectra were recorded in CH_2Cl_2 due to the presence of strong solvent bands when performed in

THF.

$Cp_2Ti(C_2Fc)_2$, $Cp*_2Ti(C_2Fc)_2$, and $^{MeOOC}Cp_2Ti(C_2Fc)_2$ The resonance Raman spectra for

$Cp_2Ti(C_2Fc)_2$ (Figure 10) are representative of all three complexes. For excitation into each

absorption band ($\lambda_{max} = 344$, 408, or 584 nm), there is significant enhancement of ν_6, the

stretching mode of the alkyne linker. Such enhancement is consistent with a change in electron

density on the Ti, resulting in a change of its valence size, in a similar fashion to the CO

symmetric stretching mode in rhenium carbonyl systems.[51-53] This suggests all transitions

involve charge transfer to Ti. Excitation into the 584 nm transition also shows enhancement of a

selection of Fc bands. The most notable are out-of-plane bending modes of the ring connected to

the alkyne bridge (ν_1 and ν_2), consistent with a change in valence size of the Fe upon oxidation.

The evidence of changes in electron density on both the Fe and Ti are consistent with the MMCT

character of this lowest energy transition. Excitation into the 408 nm band results in

enhancement of the vibrational mode ν_4, located on the C_2Cp rings of the ferrocene (C_2Cp_{Fe}).

This suggests the 408 nm transition involves LMCT character between the ferrocenyl Cp and Ti

as opposed to an LMCT transition from the titanocene Cp (Cp_{Ti}) to Ti as had been suggested

earlier.[10, 11] The fact that ν_2 also shows significant enhancement suggests some MMCT character

to this transition as well. Lastly, excitation at 351 nm results in enhancement of ν_2 and ν_4, again

suggesting a transition of mixed MMCT and LMCT character. TDDFT was performed using the

B3LYP/6-31G(d) model with a PCM assigned the macroscopic dielectric constant of CH_2Cl_2.

The assignments of transitions based on the RRS data are consistent with electron density

changes calculated from the TDDFT data (Table 5), and molecular orbital images associated
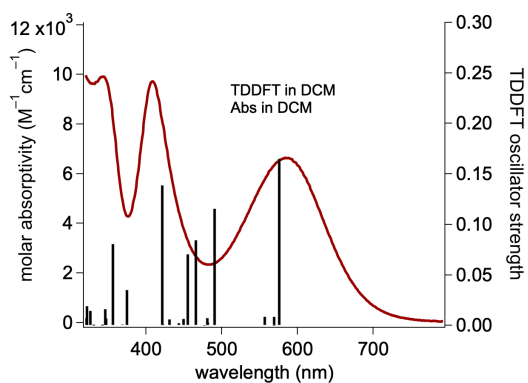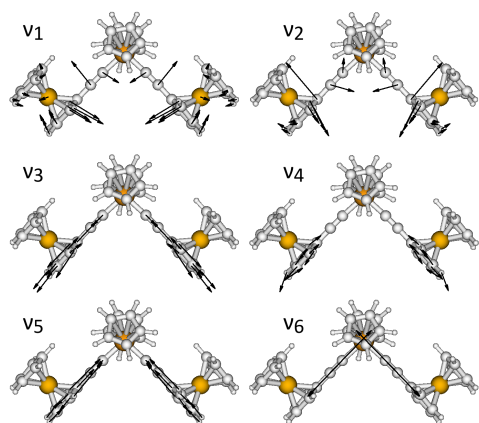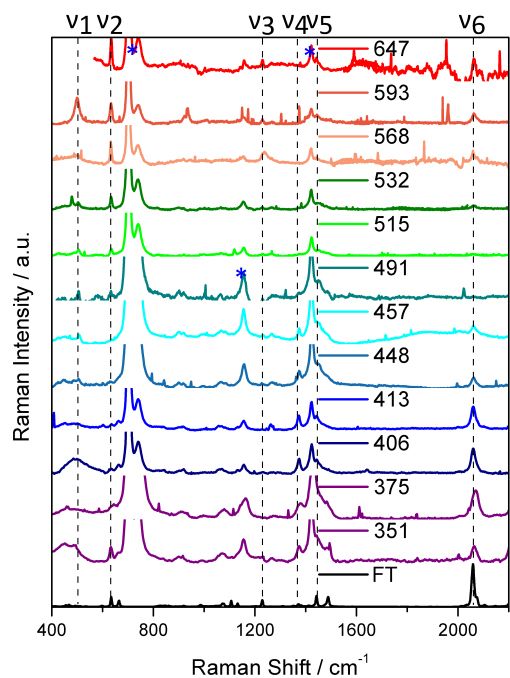
Figure 10. Top: Resonance Raman spectra for $Cp_2Ti(C_2Fc)_2$ in CH_2Cl_2, at the wavelengths listed (solvent bands are marked with *). Middle: Key vibrational modes. Bottom: Overlay of experimental UV-Vis in CH_2Cl_2 with TDDFT predicted vertical transitions. Vibrational modes and TDDFT vertical transitions modelled in CH_2Cl_2 using B3LYP/6-31G(d).

with these transitions (ESI Tables S1 and S2). Chiefly, all transitions are associated with a significant increase of electron density on Ti; the lowest energy transitions are associated with a decrease of electron density on Fe; and the highest energy transitions are associated with significant decreases in electron density on the ethynylcyclopentadienyl ligands (C_2Cp_{Fe}).

Table 5. Key electronic transitions for $Cp_2Ti(C_2Fc)_2$ with associated changes in electron density.[a]

λ (nm)	Oscillator Strength	Ti	Cp_{Ti}	Fe	C_2Cp_{Fe}	Cp_{Fe}
576	0.164	0→40 (40)	2→9 (7)	63→22 (-41)	26→23 (-3)	9→6 (-3)
491	0.115	1→25 (24)	4→5 (1)	65→38 (-27)	22→21 (-1)	8→11 (3)
422	0.139	2→55 (53)	15→10 (-5)	24→9 (-15)	53→24 (-29)	7→3 (-4)
356	0.081	6→55 (49)	6→10 (4)	17→8 (-9)	61→24 (-37)	11→2 (-9)

[a] Calculated from a Mulliken population analysis from the TDDFT data modelled with B3LYP/6-31G(d) using solvent = CH_2Cl_2. Key molecular orbitals involved in these transitions are represented in ESI Tables S1 and S2.

The corresponding RRS data for $Cp*_2Ti(C_2Fc)_2$ (ESI Figure S6) show similar features, albeit with the electronic transitions shifted to higher energy due to the increased electron density at Ti. Likewise, $^{MeOOC}Cp_2Ti(C_2Fc)_2$ shows similar features (ESI Figure S7) but with the electronic transitions shifted to lower energy due to the decreased electron density at Ti. However, it should be noted that the enhancement of the alkyne stretching mode (v_6) clearly observed in the low-energy excitations of $Cp_2Ti(C_2Fc)_2$ and $Cp*_2Ti(C_2Fc)_2$ is less pronounced for the low-energy excitation of $^{MeOOC}Cp_2Ti(C_2Fc)_2$. The assignments of transitions based on the RRS data are again consistent with electron density changes calculated from the TDDFT data (ESI Tables S3 and S4), and molecular orbital images associated with these transitions (ESI Tables S5-S8).

$Cp_2Ti(C_2Fc)_2CuI$ Upon coordination of CuI, the lowest-energy transition is red-shifted from 584 to 617 nm. However, the character of this transition remains Fe^{II} to Ti^{IV} MMCT as indicated by enhancement of v_2 and v_6 at low-energy excitations (Figure 11), consistent with the assignment of this low-energy transition based on spectroelectrochemical data.[12] Excitation into

the higher energy absorption bands using excitation wavelengths between 375 and 448 results in slight enhancement of ν_2 and ν_6 indicating these transitions have some MMCT character, however less so than the lowest-energy transition as the degree of enhancement is weaker. The TDDFT calculations (Table 6 and ESI Tables S9 and S10) are consistent with the RRS data with a transition at 586 nm dominated by Fe^{II} to Ti^{IV} MMCT. A transition at 405 nm, reveals a mix of Fe^{II} to Ti^{IV} MMCT, I to Ti^{IV} XMCT, and a smaller amount of C_2Cp_{Fe} to Ti^{IV} LMCT character. A higher-energy transition (370 nm) is dominated by I and Cu to Ti^{IV} CT character. A comparison of the TDDFT data (Tables 5 and 6) shows a significantly lower component of C_2Cp_{Fe} to Ti^{IV} LMCT for $Cp_2Ti(C_2Fc)_2CuI$ than for $Cp_2Ti(C_2Fc)_2$.

Table 6. Key electronic transitions of $Cp_2Ti(C_2Fc)_2CuI$, with associated changes in electron density.[a]

λ (nm)	Oscillator Strength	Ti	Cp_{Ti}	Fe	C_2Cp_{Fe}	Cp_{Fe}	Cu	I
586	0.127	0→39 (39)	0→9 (9)	72→15 (-57)	14→20 (6)	9→4 (-5)	3→10 (7)	1→4 (3)
504	0.051	0→22 (22)	0→5 (5)	56→35 (-21)	12→19 (7)	7→10 (3)	4→6 (2)	19→2 (-17)
405	0.156	0→49 (49)	2→9 (7)	36→4 (-32)	30→19 (-11)	7→1 (-6)	5→13 (8)	20→5 (-15)
370	0.237	1→49 (38)	2→9 (7)	9→4 (-5)	18→19 (1)	1→1 (0)	25→13 (-12)	34→5 (-29)

[a] Calculated from a Mulliken population analysis from the TDDFT data modelled with B3LYP/6-31G(d)/LANL2DZ on I using solvent = CH_2Cl_2. Key molecular orbitals involved in these transitions are represented in ESI Tables S9 and S10.

Compared to $Cp_2Ti(C_2Fc)_2$, $Cp^*_2Ti(C_2Fc)_2$ and $^{MeOOC}Cp_2Ti(C_2Fc)_2$, the alkyne asymmetric and symmetric stretching modes (ν_{6a} and ν_{6b}) of $Cp_2Ti(C_2Fc)_2CuI$ are well-resolved with an energy separation of 35 cm^{-1}. Excitation into the lowest-energy absorption band results in selective enhancement of the symmetric mode (ν_{6b}). This is significant because the enhancement of a mode in which both alkyne linkers are in phase is consistent with an electronic transition in which the distortion along those two linkers is the same – i.e., in which the donor MO is delocalized across both units.[50] This delocalized donor MO as part of the MMCT transition is supported by the TDDFT calculations.
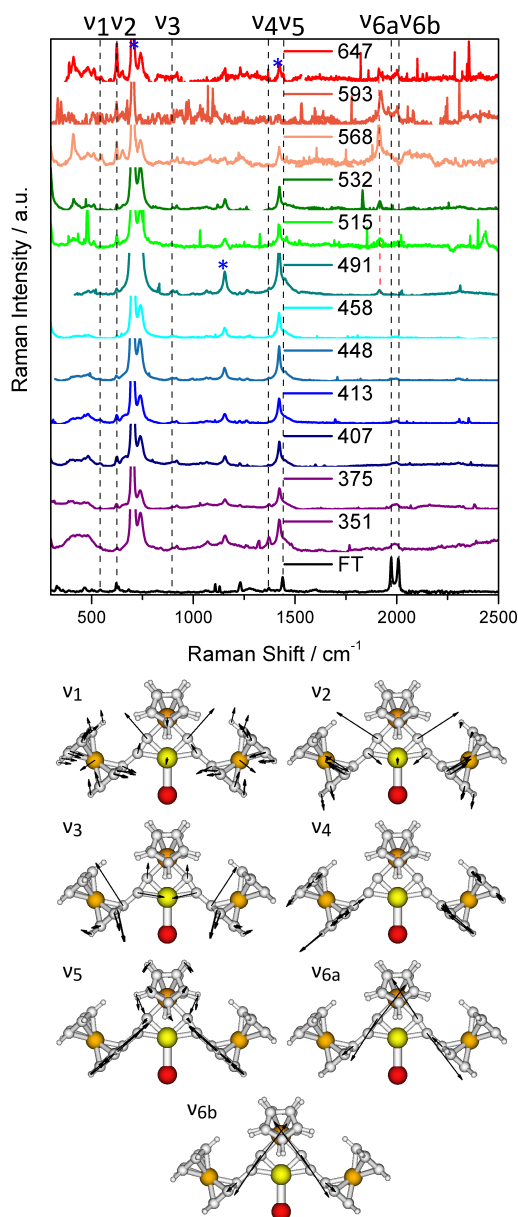
Figure 10. Top: Resonance Raman spectra for Cp₂Ti(C₂Fc)₂CuI in CH₂Cl₂, at the wavelengths listed (solvent bands are marked with *). Middle: Key vibrational modes. Bottom: Overlay of experimental UV-Vis in CH₂Cl₂ with TDDFT predicted vertical transitions. Vibrational modes and TDDFT vertical transitions modelled in CH₂Cl₂ using B3LYP/6-31G(d) with LANL2DZ ECP on I.

Conclusions

In summary, a series of complexes with low-energy Fe^{II} to Ti^{IV} MMCT transitions was investigated using solvatochromism and RRS augmented with TDDFT calculations in order to interrogate the nature of the CT transitions. In addition to supporting prior characterizations that the lowest-energy transition involves significant Fe^{II} to Ti^{IV} MMCT character, the combination of these techniques has revealed several additional features. First, it is noteworthy that the minimum energy conformation of $^{MeOOC}Cp_2Ti(C_2Fc)_2$, as predicted by DFT, is not sufficient to predict dipole moment changes that are qualitatively consistent with experimental results. This highlights the need to consider multiple rotational conformations when using DFT/TDDFT to predict experimental properties when such rotamers are accessible. Second, a combination of RRS and TDDFT has also provided a better understanding of the higher-energy transitions. Chiefly, for $Cp_2Ti(C_2Fc)_2$, $Cp^*_2Ti(C_2Fc)_2$ and $^{MeOOC}Cp_2Ti(C_2Fc)_2$, these higher-energy transitions appear to be a mixture of MMCT and ethynylcyclopentadienyl to Ti^{IV} LMCT, as opposed to Cp_{Ti} to Ti^{IV} MMCT as previously suggested. For $Cp_2Ti(C_2Fc)_2CuI$, the TDDFT analysis suggests these higher energy transitions also have significant I to Ti XMCT and a mixture of Fe and Cu to Ti MMCT character. Lastly, investigations into the lowest-energy absorption band of $Cp_2Ti(C_2Fc)_2CuI$ suggest it retains its Fe^{II} to Ti^{IV} MMCT character despite the coordination of CuI. Furthermore, excitation into this band results in selective enhancement of the symmetric alkynyl stretching mode, consistent with a donor MO that is delocalized across both ethynylferrocene ligands, in accord with the TDDFT / solvatochromism investigations.

Conflicts of Interest

There are no conflicts of interest to declare.

References

1. Mishra, A.; Fischer, M. K. R.; Bäuerle, P. *Angew. Chem., Int. Ed.* **2009**, *48*, 2474-2499.

2. Mathew, S.; Yella, A.; Gao, P.; Humphry-Baker, R.; Curchod, B. F. E.; Ashari-Astani, N.; Tavernelli, I.; Rothlisberger, U.; Nazeeruddin, M. K.; Grätzel, M. *Nat. Chem* **2014**, *6*, 242-247.

3. Hardin, B. E.; Snaith, H. J.; McGehee, M. D. *Nat. Photonics* **2012**, *6*, 162-169.

4. Liang, M.; Chen, J. *Chem. Soc. Rev.* **2013**, *42*, 3453-3488.

5. Di Bella, S.; Dragonetti, C.; Pizzotti, M.; Roberto, D.; Tessore, F.; Ugo, R. *Top. Organomet. Chem* **2010**, *28*, 1-55.

6. Green, K. A.; Cifuentes, M. P.; Samoc, M.; Humphrey, M. G. *Coord. Chem. Rev.* **2011**, *255*, 2530-2541.

7. Salman, S.; Brédas, J.-L.; Marder, S. R.; Coropceanu, V.; Barlow, S. *Organometallics* **2013**, *32*, 6061-6068.

8. Barlow, S.; Marder, S. R. *Chem. Comm.* **2000**, 1555-1562.

9. Parker, T. C.; Marder, S. R. *Synthetic Methods in Organic Electronic and Photonic Materials, a Practical Guide*; Royal Society of Chemistry: Cambridge UK, 2015.

10. Turlington, M. D.; Pienkos, J. A.; Carlton, E. S.; Wroblewski, K. N.; Myers, A. R.; Trindle, C. O.; Altun, Z.; Rack, J. J.; Wagenknecht, P. S. *Inorg. Chem.* **2016,** *55*, 2200-2211.

11. Livshits, M. Y.; Turlington, M. D.; Trindle, C. O.; Wang, L.; Altun, Z.; Wagenknecht, P. S.; Rack, J. J. *Inorg. Chem.* **2019**, *58*, 15320-15329.

12. Pienkos, J. A.; Webster, A. B.; Piechota, E. J.; Agakidou, A. D.; McMillen, C. D.; Pritchett, D. Y.; Meyer, G. J.; Wagenknecht, P. S. *Dalton Trans.* **2018**, *47*, 10953-10964.

13. Pienkos, J. A.; Agakidou, A. D.; Trindle, C. O.; Herwald, D. W.; Altun, Z.; Wagenknecht, P. S. *Organometallics* **2016**, *35*, 2575-2578.

14. Suppan, P. *J. Photochem. Photobiol., A: Chem.* **1990**, *50*, 293-330.

15. Marini, A.; Muñiz-Losa, A.; Biancardi, A.; Mennucci, B. *J. Phys. Chem. B* **2010**, *114*, 17128-17135.

16. (a) Kamlet, M. J.; Abboud, J. L.; Taft, R. W. *J. Am. Chem. Soc.* **1977**, *99*, 6027-6038. (b) Kamlet, M.; Abboud, J.-L. M.; Abraham. M. H.; Taft, R. W. *J. Org. Chem.* **1983**, *48*, 2877-2887.

17. (a) Catalán, J. *J. Phys. Chem. B* **2009**, *113*, 5951-5960. (b) Catalán, J., Hopf, H. *Eur. J. Org. Chem.* **2004**, 4694-4702.

18. Clark, R. J. H.; Dines, T. J. *Angew. Chem. Int. Ed. Eng.* **1986**, *25*, 131-158.

19. Wächtler, M.; Guthmuller, J.; González, L.; Dietzek, B. *Coord. Chem. Rev.* **2012**, *256*, 1479-1508.

20. Horvath, R.; Huff, G. S.; Gordon,, K. C.; George, M. W. *Coord. Chem. Rev.* **2016**, *325*, 41-58.

21. Myers, A. B. *Acc. Chem. Res.* **1997**, *30*, 519-527.

22. Barnsley, J. E.; Lomax, B. A.; McLay, J. R. W.; Larson, C. B. Lucas, N. T.; Gordon, K. C. *ChemPhotoChem* **2017**, *1*, 432-441.

23. Mapley, J. I.; Ross, D. A. W.; McAdam, C. J.; Gordon, K. C.; Crowley. J. D. *J. Coord. Chem.* **2019**, *72*, 1378-1394.

24. (a) Sutton, J. J.; Nguyen, T. L.; Woo, H. Y.; Gordon, K. C. *Chem. Asian J.* **2019**, *14*, 1175-1183. (b) Mapley, J. I.; Hayes, P.; Officer, D. L.; Wagner, P.; Gordon, K. C. *J. Phys. Chem. A* **2020**, *124*, 5513-5522. (c) Shillito, G. E.; Hall, T. B. J.; Preston, D.; Traber, P.; Wu, L.; Reynolds, K. E. A.; Horvath, R.; Xun, X. Z.; Lucas, N. T.; Crowley, J. D.; George, M. W.; Kupfer, S.; Gordon, K. C. *J. Am. Chem. Soc.* **2018**, *140*, 4534-4542.

25. Frisch, M. J.; Trucks, G. W.; Schlegel, H. B.; Scuseria, G. E.; Robb, M. A.; Cheeseman, J. R.; Scalmani, G.; Barone, V.; Petersson, G. A.; Nakatsuji, H.; Li, X.; Caricato, M.; Marenich, A. V.; Bloino, J.; Janesko, B. G.; Gomperts, R.; Mennucci, B.; Hratchian, H. P.; Ortiz, J. V.; Izmaylov, A. F.; Sonnenberg, J. L.; Williams-Young, D.; Ding, F.; Lipparini, F.; Egidi, F.; Goings, J.; Peng, B.; Petrone, A.; Henderson, T.; Ranasinghe, D.; Zakrzewski, V. G.; Gao, J.; Rega, N.; Zheng, G.; Liang, W.; Hada, M.; Ehara, M.; Toyota, K.; Fukuda, R.; Hasegawa, J.; Ishida, M.; Nakajima, T.; Honda, Y.; Kitao, O.; Nakai, H.; Vreven, T.; Throssell, K.; Montgomery, J. A., Jr.; Peralta, J. E.; Ogliaro, F.; Bearpark, M. J.; Heyd, J. J.; Brothers, E. N.; Kudin, K. N.; Staroverov, V. N.; Keith, T. A.; Kobayashi, R.; Normand, J.; Raghavachari, K.; Rendell, A. P.; Burant, J. C.; Iyengar, S. S.; Tomasi, J.; Cossi, M.; Millam, J. M.; Klene, M.; Adamo, C.; Cammi, R.; Ochterski, J. W.; Martin, R. L.; Morokuma, K.; Farkas, O.; Foresman, J. B.; Fox, D. J. *Gaussian 16*, Revision C.01; Gaussian, Inc., Wallingford CT, 2016.

26. Dennington, R.; Keith, T. A.; Millam, J. M. *GaussView*, Version 6; Semichem Inc., Shawnee Mission, KS, 2016.

27. Boyle, N. M.; Tenderholt, A. L.; Langner, K. M. *J. Comp. Chem.* **2008**, *29*, 839-845

28. Tomasi, J.; Mennucci, B; Cammi, R. *Chem. Rev.* **2005**, *105*, 2999-3093.

29. Salzner, U. *J. Chem. Theory. Comput.* **2013**, *9*, 4064-4073.

30. Niehaus, T. A.; Hofbeck, T.; Yersin, H. *RSC Adv.* **2015**, *5*, 63318 – 63329.

31. Marcus, Y. *Chem. Soc. Rev.* **1993**, *22*, 409-416.

32. Kosower, E. M. *J. Am. Chem. Soc.* **1958**, *80*, 3253-3260.

33. (a) Cerón-Carrasco, J. P.; Jacquemin, D.; Laurence, C.; Planchat, A.; Reichardt, C.; Sraïdi, K. *J. Phys. Org. Chem.* **2014**, *27*, 512-518. (b) Dimroth, K.; Reichardt, C.; Siepmann, T.; Bohlmann, F. *Justus Liebigs Ann. Chem.* **1963**, *661*, 1-37.

34. Swain, C. G.; Swain, M. S.; Powell, A. L.; Alunni, S. *J. Am. Chem. Soc.* **1983**, *105*, 502-513.

35. Catalán, J., Del Valle, J. C. *J. Phys. Chem. B* **2014**, *118*, 5168-5176.

36. Holm, C. H.; Ibers, J. A. *J. Chem. Phys.* **1959**, *30*, 885-888.

37. Winter, C. H.; Dobbs, D. A.; Zhou, X.-X. *J. Organomet. Chem.* **1991**, *403*, 145-151.

38. Lang, H.; Herres, M.; Zsolnai, L. *Organometallics* **1993**, *12*, 5008 - 5011.

39. Wodrich, M. D.; Corminboeuf, C.; Schleyer, P. *Org. Lett.* **2006**, *8*, 3631-3634.

40. Barlow, S.; Bunting, H. E.; Ringham, C.; Green, J. C.; Bublitz, G. U.; Boxer, S. G.; Perry, J. W.; Marder, S. R. *J. Am. Chem. Soc.* **1999**, *121*, 3715-3723.

41. (a) Huesmann, H.; Förster, C.; Siebler, D.; Gasi, T.; Heinze, K. *Organometallics* **2012**, *31*, 413-427. (b) Warratz, R.; Peters, G.; Studt, F.; Römer, R.-H.; Tuczek, F. *Inorg. Chem.* **2006**, *45*, 2531-2542.

42. Alain, V.; Fort, A.; Barzoukas, M.; Chen, C.-T.; Blanchard-Desce, M.; Marder, S. R.; Perry, J. W. *Inorg. Chim. Acta* **1996**, *242*, 43-49.

43. Laus, G.; Strasser, C. E.; Holzer, M.; Wurst, K.; Pürstinger, G.; Ongania, K.-H.; Rauch, M.; Bonn, G.; Schottenberger, H. *Organometallics* **2005**, *24*, 6085-6093.

44. Barlow, S. *Inorg. Chem.* **2001**, *40*, 7047-7053.

45. Ratera, I.; Sporer, C.; Ruiz-Molina, D.; Ventosa, N.; Baggerman, J.; Brouwer, A. M.; Rovira, C.; Veciana, J. *J. Am. Chem. Soc.* **2007**, *129*, 6117-6129.

46. Laus, G.; Schottenberger, H.; Wurst, K.; Herber, R. H.; Griesser, U. *J. Phys. Chem. B* **2004**, *108*, 5082-5087.

47. Nemykin, V. N.; Maximov, A. Y.; Koposov, A. Y. *Organometallics* **2007**, *26*, 3138-3148.

48. Nemykin, V. N.; Makarova, E. A.; Grosland, J. O.; Hadt, R. G.; Koposov, A. Y. *Inorg. Chem.* **2007**, *46*, 9591-9601.

49. Speck, J. M.; Korb, M.; Schade, A.; Spange, S.; Lang, H. *Organometallics* **2015**, *34*, 3788-3798.

50. Da Re, R. E.; Jantunen, K. C.; Golden, J. T.; Kiplinger, J. L.; Morris, D. E. *J. Am. Chem. Soc.* **2005**, *127*, 682-689.

51. Horvath, R.; Fraser, M. G.; Cameron, S. A.; Blackman, A. G.; Wagner, P.; Officer, D. L.; Gordon, K. C. *Inorg. Chem.* **2013**, *52*, 1304-1317.

52. Horvath, R.; Otter, C. A.; Gordon, K. C.; Brodie, A. M.; Ainscough, E. W. *Inorg. Chem.* **2010**, *49*, 4073-4083.

53. Smothers, W. K.; Wrighton, M. S. *J. Am. Chem. Soc.* **1983**, *105*, 1067-1069.